Video Article

Development of an Electrochemical DNA Biosensor to Detect a Foodborne Pathogen

Noordiana Nordin[1], Nor Azah Yusof[2,3], Son Radu[1], Roozbeh Hushiarian[4]

[1]Laboratory of Food Safety and Food Integrity, Institute of Tropical Agriculture and Food Security, Universiti Putra Malaysia

[2]Laboratory of Functional Device, Institute of Advanced Technology, Universiti Putra Malaysia

[3]Department of Chemistry, Faculty of Science, Universiti Putra Malaysia

[4]La Trobe Institute for Molecular Science, La Trobe University

Correspondence to: Noordiana Nordin at noordiana@upm.edu.my, Roozbeh Hushiarian at r.hushiarian@latrobe.edu.au

URL: https://www.jove.com/video/56585
DOI: doi:10.3791/56585

Keywords: Bioengineering, Issue 136, Polylactic acid-stabilized gold nanoparticles, screen-printed carbon electrode, DNA biosensor, Vibrio parahaemolyticus, Electrochemical sensor, DNA hybridization

Date Published: 6/3/2018

Citation: Nordin, N., Yusof, N.A., Radu, S., Hushiarian, R. Development of an Electrochemical DNA Biosensor to Detect a Foodborne Pathogen. *J. Vis. Exp.* (136), e56585, doi:10.3791/56585 (2018).

Abstract

Vibrio parahaemolyticus (V. parahaemolyticus) is a common foodborne pathogen that contributes to a large proportion of public health problems globally, significantly affecting the rate of human mortality and morbidity. Conventional methods for the detection of *V. parahaemolyticus* such as culture-based methods, immunological assays, and molecular-based methods require complicated sample handling and are time-consuming, tedious, and costly. Recently, biosensors have proven to be a promising and comprehensive detection method with the advantages of fast detection, cost-effectiveness, and practicality. This research focuses on developing a rapid method of detecting *V. parahaemolyticus* with high selectivity and sensitivity using the principles of DNA hybridization. In the work, characterization of synthesized polylactic acid-stabilized gold nanoparticles (PLA-AuNPs) was achieved using X-ray Diffraction (XRD), Ultraviolet-visible Spectroscopy (UV-Vis), Transmission Electron Microscopy (TEM), Field-emission Scanning Electron Microscopy (FESEM), and Cyclic Voltammetry (CV). We also carried out further testing of stability, sensitivity, and reproducibility of the PLA-AuNPs. We found that the PLA-AuNPs formed a sound structure of stabilized nanoparticles in aqueous solution. We also observed that the sensitivity improved as a result of the smaller charge transfer resistance (R_{ct}) value and an increase of active surface area (0.41 cm^2). The development of our DNA biosensor was based on modification of a screen-printed carbon electrode (SPCE) with PLA-AuNPs and using methylene blue (MB) as the redox indicator. We assessed the immobilization and hybridization events by differential pulse voltammetry (DPV). We found that complementary, non-complementary, and mismatched oligonucleotides were specifically distinguished by the fabricated biosensor. It also showed reliably sensitive detection in cross-reactivity studies against various food-borne pathogens and in the identification of *V. parahaemolyticus* in fresh cockles.

Video Link

The video component of this article can be found at https://www.jove.com/video/56585/

Introduction

A major topic of public and scientific debate in recent years, food poisoning is mainly associated with 3 agents: microorganisms[1], chemicals[2], and parasites[3]. Contaminated food can cause serious health consequences in humans, especially in the higher risk group of those with weak immune systems, the elderly, pregnant women, babies, and young children[4]. With more than a million cases of acute diarrhea occurring annually in children under 5 years old in Africa, Asia, and Latin America, food poisoning is a major global disease[5,6] and the World Health Organization has established microorganisms as the most important contributor[7]. *Vibrio parahaemolyticus* stands out amongst the most widely recognized virulent strains. Usually found in coastal, estuarine, and marine environments[8], it is a Gram-negative bacterium, which becomes active in high salt environments, and causes serious human gastroenteritis when eaten in inadequately cooked, mishandled or raw marine products[9]. Additionally, existing medical conditions in some people make them prone to wound infection, septicemia or ear infection arising from *V. parahaemolyticus*[10]. The virulence factors of *V. parahaemolyticus* hemolysins are divided into two types which contribute to the disease pathogenesis: thermostable direct hemolysin (TDH) coded by tdh genes, and TDH-related hemolysin coded by trh genes[11]. The virulence markers (tdh and trh genes) of *V. parahaemolyticus* are mostly found in clinical specimens rather than in environmental specimens.

V. parahaemolyticus possesses the ability to survive under a broad range of conditions, rapidly responding to environmental changes[12]. Its proliferation mechanism escalates its hazard potential as its toxicity increases in parallel with cell mass[13]. Even worse, climate change is providing these bacteria with ample conditions to accelerate their cell population growth[14]. Due to its high frequency, *V. parahaemolyticus* needs to be monitored along the food supply chain, particularly in the trade and production of seafood since those products are where they are found in enormous quantities[15,16] throughout the world. Currently the bacteria are identified and isolated using a range of methods including biochemical tests, enrichment and selective media[17], enzyme-linked immunomagnetic sorbent assay (ELISA)[18], pulse-field gel electrophoresis (PFGE)[19], latex agglutination tests, and polymerase chain reaction (PCR) tests[20]. These methods usually require qualified personnel, sophisticated

instruments, and laborious techniques which do not provide information about contamination immediately. This severely limits the likelihood of promptly detecting harmful contamination and on-site applications. Rapid detection tools remain an outstanding challenge.

Biosensing is emerging as a promising option for the detection of foodborne pathogens because it offers a time-saving, cost-effective, practical, and real-time analysis method[21,22,23,24]. However, although there have been many positive results of analyte detection in spiked samples and standard solution using biosensors, there is still a lack of research applied to real samples either in aqueous mixtures or organic extracts[25]. Recently, electrochemical biosensors using direct and/or indirect deoxyribonucleic acid (DNA) detection have received increased attention among scientists, due to their specific detection of the complementary target via a hybridization event[26,27,28,29]. These unique approaches are more stable in comparison with enzyme-based biosensors, thus offering a promising technology for miniaturization and commercialization. The target of the study reported here is to construct a fast tool that can detect *V. parahaemolyticus* with high selectivity, sensitivity, and practicality, based on the DNA sequence specificity during hybridization. Identification strategies involve the combination of polylactic acid-stabilized gold nanoparticles (PLA-AuNPs)[30] and screen-printed carbon electrodes (SPCEs) in the presence of the hybridization indicator, methylene blue (MB). The potential of the developed detection construct is further explored using bacteria DNA lysate and fresh cockle samples.

Protocol

NOTE: All the chemical and biochemical reagents to be used should be of analytical grade and used without further purification. Prepare all solutions using sterile deionized water. Autoclave all glassware prior to sterilization.

Caution: Please use all appropriate safety practices when performing laboratory activities including the use of engineering controls (fume hood, glovebox) and personal protective equipment (safety glasses, gloves, lab coat, full length pants, closed-toe shoes).

1. Fabrication and Characterization of Modified Electrode using PLA-AuNPs

1. **Preparation and characterization of PLA-AuNPs**
    1. Quickly add 10 mL of sodium citrate solution (38.8 mM) to 100 mL of boiling aqueous chloroauric acid solution (1 mM) and cool it down to ambient temperature. Observe the changes in color in the prepared AuNPs solution which starts as yellow, changes to blackish and finally ends as dark ruby red.
    2. Place the PLA pellets in a stainless-steel mold for the melting process and preheat them at a temperature of 190 °C for 10 min. Follow with the pressing procedure: put them under a pressure of 2.2 MPa for 1 min as part of the PLA sheet preparation. The PLA sheet will be ready for use after cooling for about 3 h.
    3. Stirring vigorously, dissolve 0.68 mg of the PLA sheets in 5 mL of chloroform at room temperature. Mix the dissolved PLA with 10 mL of the previously prepared AuNPs solution and homogeneously stir it at room temperature. The homogeneous mixtures can then be denoted as PLA-AuNPs and characterized using UV-Vis, XRD, TEM, and FESEM with EDX.

2. **Preparation and characterization of modified screen-printed carbon electrode**
NOTE: The SPCE used in this study comprises a three-electrode system: a counter electrode, a carbon working electrode, and an Ag/AgCl reference electrode.
    1. Quickly pipette 25 µL of the homogenous solution of PLA-AuNPs onto the SPCE and then air dry it for 24 h prior to use.
    2. Electrochemically characterize the modified electrodes, SPCE/PLA-AuNPs, in potassium ferro cyanide ($K_3[Fe(CN)_6]^{3-/4-}$) to measure active surface area, electrochemical impedance spectroscopy, repeatability, reproducibility, and stability[30].

2. Development of the Electrochemical DNA Biosensor

1. **Probe preparation**
Note: The sequences of the ssDNA probe and complementary DNA were chosen based on information from the National Center for Biotechnology Information (NCBI) database.
    1. Purchase synthetic oligonucleotides (20-mer ssDNA probe, 20-mer complementary DNA, 20-mer mismatched DNA, and 21-mer non-complementary DNA) as lyophilized powder from commercial laboratories, based on the following sequences:
thiolated ssDNA probe: 5′- / 5ThioMC6-D/CGGATTATGCAGAAGCACTG - 3′
complementary DNA: 5′ - CAGTGCTTCTGCATAATCCG - 3′
one-base mismatched DNA: 5′ - CAGTGCTTCTGC ṪTAATCCG - 3′
three-base mismatched DNA: 5′ - CAGTGCTTCT Ċ ṪṪAATCCG - 3′
non-complementary DNA: 5′ - CGCACAAGGCTCGACGGCTGA - 3′
    2. Prepare stock solutions of all oligonucleotides (100 µM) using a sterile TE solution (10 mM Tris-HCl, 1 mM EDTA, pH 7.5), divided into analytical portions. Keep this at -4 °C and then make the appropriate dilutions just prior to use.

2. **Optimization of Immobilization and Hybridization**
Note: An SPCE modified with PLA-AuNPs, denoted as SPCE/PLA-AuNPs, was used for this study and a drop casting method was used for the DNA immobilization and hybridization.
    1. First, immobilize 25 µL of thiolated ssDNA probe on the SPCE/PLA-AuNPs and then air dry it for 24 h at room temperature, after which it will be finally denoted as SPCE/PLA-AuNPs/ssDNA. Determine optimization of the immobilization condition by using three factors: the concentration of ssDNA (ranging from 0.2 to 1.4 µM), time (ranging from 30 to 210 min), and temperature (ranging from 25 to 75 °C).
    2. Pipette 25 µL of the complementary DNA on to the surface of SPCE/PLA-AuNPs/ssDNA to carry out the hybridization event after which it can be finally denoted as SPCE/PLA-AuNPs/dsDNA. Determine optimization of the hybridization condition via the two factors of time (ranging from 5 to 30 min) and temperature (ranging from 25 to 75 °C).

3. Immerse the immobilized and hybridized electrodes in 20 µM MB for 30 min. Remove the non-specifically adsorbed DNA and excess MB by washing with 0.5 M ABS/20 mM NaCl (pH 4.5) and then rinsing with deionized water. Measure the peak current of MB reduction using DPV technique. Execute the DPV measurement using 0.1 M PBS (pH 7) containing no indicator.

3. **Characterization of the fabricated DNA biosensor**
   1. Immerse the SPCE/PLA-AuNPs in 20 µM MB for 30 min, wash with 0.5 M ABS/20 mM NaCl (pH 4.5), and then rinse with deionized water prior to measuring. Follow a similar procedure for all interactions including the probe DNA, complementary DNA, mismatched DNA, and non-complementary DNA samples.
   2. Measure the electrochemical reduction.
      NOTE: We measured DPV using a commercially manufactured Autolab with interface software.
      The DPV measurements of the MB electrochemical reduction performed at a potential ranging from -0.5 V to 0.25 V, with a step potential of 0.005 V, modulation amplitude of 0.05 V, and a scan rate of 7.73 mVs^{-1} in 0.1 M PBS (pH 7), containing no indicator. The selectivity, sensitivity, reproducibility, and heat stability of the fabricated DNA biosensor were further studied. Reported results were presented as mean value measurements in three replicates.

3. Validation of the Fabricated DNA Biosensor Using Real Samples

1. **Preparation of bacterial strains**
   1. Select bacterial samples based on their significant contamination of seafood[31,32] .
      NOTE: *V. parahaemolyticus* as reference strains and 8 other bacterial strains (*Campylobacter jejuni*, *Listeria monocytogenes*, *Salmonella typhimurium*, *Salmonella enteritis*, *Klebsiella pneumonia, Escherichia coli O157:H7*, *Bacillus cereus*, and *Vibrio alginolyticus*) of the common foodborne pathogen were employed for the electrochemical DNA biosensor validation in this study.
   2. Conduct a routine sub-culture of bacterial strains on their respective agar every two weeks to maintain their viability, refer **Table 1** for culture conditions.
   3. Maintain long-term preservation of the bacterial strains in their respective growing broths containing 20% (v/v) glycerol at -80 °C as glycerol protects bacteria by preventing the formation of ice crystals that can damage them during the freezing process. Next, inoculate a loop of preserved bacterial cell culture in glycerol stocks into the respective broths. Incubate the broths according to their respective growth time and temperature when needing to revive the bacteria.
   4. Determine the quantity of *V. parahaemolyticus* cells using a spread plate technique[33], a standard and a well-known method for enumerating microorganisms derived from a series of dilutions.
      1. Culture *V. parahaemolyticus* in Trypticase Soy Broth (TSB + 3% NaCl) at 37 °C in a 140-rpm shaking condition. Then, transfer 1 mL of the bacteria cell culture into 9 mL of TSB + 3% NaCl to obtain a 10^{-1} dilution factor.
   5. Repeat this step nine times to get a full series of up to 10^{-10} dilution factor. Next, spread 0.1 mL of each dilution factor (starting from 10^{-1} to 10^{-10}) on a Vibrio's selective agar plate for colony counting, respectively. Incubate the plates incubated at 37 °C for 24 h.
   6. Use a colony counter to count individual colonies and then back-calculate (count the CFU/pipetted amount x dilution factor) to get a colony-forming unit per milliliter density (CFU mL^{-1}). Derive the concentration of the colony forming units (CFUs) in the bacteria cell suspensions from the calibration plot of CFU mL^{-1} against absorbance.

2. **Preparation of the PCR assay**
   1. Extract genomic DNA following a modified boiled lysis procedure[34]. First, streak an individual bacterial strain on agar media and inoculate it in broth media, followed by incubating it at its relative growth condition, a 140 rpm shaking condition.
   2. Pipette a 1 mL culture of broth into a micro centrifuge tube. Centrifuge this at 4830 x g and 4 °C for 1 min to obtain pellets. Use about 500 µL of sterile TE buffer for re-suspension with the pellet. Hold the resulting suspension for 10 min at 98 ± 2 °C in a heating block and immediately chill it at -18 °C for 10 min to lyse the cells and release the DNA.
   3. Centrifuge the genomic DNA at 4830 x g and 4 °C for 3 min to obtain a clear suspension and keep the supernatant at -20 °C for further use. Use a biophotometer measurement with UV absorption at a wavelength of 260 nm (as nucleic acids absorbing wavelength of light) and also at a wavelength of 280 nm (as the proteins absorbing wavelength of light) to determine the concentration and purity of the extracted genomic DNA and then identify all strains using standard biochemical assays[35] and verifying them by 16S rRNA gene sequencing[36]. Finally, denature the genomic DNA at 92 °C for 2 min and cool it rapidly in ice water prior to application to the biosensor.
   4. Further confirm the presence *V. parahaemolyticus* using PCR to target the toxR gene. Perform this procedure in a thermocycler using a primer pair (5'-GTCTTCTGACGCAATCGTTG-3' and 5'-ATACGAGTGGTTGCTGTCATG-3'). Optimize the PCR amplification in a total reaction volume of 25 µL consisting of sterile water (15.5 µL), buffer (5 µL), primer (1 µL, 10 µM), dNTP mix (1 µL), DNA template (2 µL), and Taq DNA polymerase (0.2 µL, 10x).
   5. Mix the components well and arrange the PCR amplification of the target sequence in a thermocycler programmed for 30 cycles of amplification. In our study, each cycle consisted of three-step reactions *i.e.*, initial denaturation (94 °C, 3 min) followed by 30 cycles of denaturation (94 °C, 1 min), annealing (63 °C, 1.5 min) and extension (72 °C, 1.5 min), followed by final extension (72 °C, 7 min).
   6. Determine the amplified products and their sizes via electrophoresis on 1.5% agarose gel. Capture the gel images with a commercially produced gel-documentation system.

3. **Preparation of cockle samples**
   1. Obtain fresh samples.
      NOTE: Our fresh cockles (*Anadara granosa*) were obtained from the wet market in Serdang, Selangor, and quickly brought to the laboratory in an ice cooler box for analysis. Divide the samples into 2 groups, namely the treated and untreated group, assuming that the cockles were harvested uniformly from the start of the harvest until placing them into cold storage.
   2. Pre-treat cockles in the treated group by storing them at -20 °C for 24 h, followed by exposure to UV light at 20 °C for 4 h prior to DNA extraction.
      NOTE: The freezing temperature and UV exposure used for the controlled group kills or at least limits the naturally accumulating *V. parahaemolyticus* in the cockles. Do not apply a higher pasteurization regime of 70 °C as the aim of the controlled condition in this

study is to mimic the actual situation of the fresh cockles. Meanwhile, analyze samples directly from the untreated group without any pre-treatment as soon as they arrive in the laboratory.

3. Subculture a strain of *V. parahaemolyticus* ATCC 17802 in TSB (3% NaCl). Determine the level of viable cells in the inoculum via plating of appropriate dilutions of TSB (3% NaCl) on CA in order to obtain an inoculum of 10^4 CFU mL^{-1} of *V. parahaemolyticus*. Wash each cockle in distilled water and scrub it free of dirt before using sterile forceps in a laminar flow cabinet to remove the tissues from the shell.
4. Homogenize about 10 g of cockle tissue samples with a homogenizer in 90 mL of sterile TSB (3% NaCl) for 60 s. Add a known amount of *V. parahaemolyticus* to 9 mL of the homogenized sample broth for the spiked samples. Use the unspiked samples as a negative control. Estimate the cell counts of *V. parahaemolyticus* spiked on to the cockle samples by plating 0.1 mL of the samples on CA, and subsequently, pipetting 1 mL of samples into a microcentrifuge tube for DNA sample extraction, to be used in the biosensor and PCR assay.
5. Extract the genomic DNA of the *V. parahaemolyticus* from the spiked and unspiked samples following a modified boiled lysis procedure[36]. Finally, determine the DNA concentration and purity using a bio photometer measurement with UV absorption at a wavelength of 260 nm (as nucleic acids absorbing wavelength of light) and also at a wavelength of 280 nm (as the proteins absorbing wavelength of light).

Representative Results

Formation of AuNPs was revealed through the change in color of the aqueous solution with sodium citrate present. This caused the color to change from light yellow to a deep ruby red. The generation of PLA-AuNPs was confirmed from the UV-vis spectra (**Figure 1**) where the growth of the surface plasmon resonance (SPR) peak was found at around 540 nm. The formation and existence of PLA-AuNPs was indicated at 500-600 nm wavelength ranges, depending on particle size[37]. The XRD patterns of AuNPs and PLA-AuNPs are shown in **Figure 2**. All crystallite peaks were observed at the 2θ of 31.7, 38.2, 44.4, 64.7, and 77.7°. They were attributed to the (100) (111) (200) (220), and (311) crystallographic planes of cubic-FCC (face-centered cubic) gold (metal) nanostructures (JCPDS file no.-00-004-0783). The PLA-AuNPs crystallite peak intensities also increased as a broader diffraction peak centered at 31.7°, implying that the AuNPs were embedded in the PLA and suggesting the formation of polyphasic gold nanostructures[38]. Furthermore, all AuNP diffraction peaks shown on the PLA-AuNPs indicated that the AuNPs had a stable structure. The mean size of PLA-AuNPs was calculated using Scherrer's equation ($L = k\lambda/\beta\cos\theta$), by determining the width of the (100) Bragg's reflection. From the FWHM and d-spacing (**Table 2**), the crystallite size of PLA-AuNPs was calculated as 27 nm.

The dimensions of the PLA-AuNPs and its morphology were further investigated using TEM. From the TEM particle distribution curve and images of PLA-AuNPs, it was seen that gold nanoparticles were almost spherical in shape (**Figure 3**). The size of the nanoparticles was in the range of about 37 nm, slightly bigger than obtained from Scherrer's formula, suggesting a polycrystalline nature of the as-synthesized nanoparticles[39]. Smaller size resulting from XRD in contrast to TEM has also been observed in previous research, most likely because the particle structure is polycrystalline in nature because of the significant amount of crystallites that are smaller (sub-particles)[40]. **Figure 4** shows the FESEM image of as-prepared PLA-AuNPs on SPCE. It is evident from the FESEM images and EDX spectra that the SPCE/PLA-AuNPs had the highest weight percentage of gold, greatest density, and largest surface of nanoparticle coverage. It can also be noted, particularly, that **Figure 4**(**a**) shows the FESEM image of a bare SPCE. The FESEM image in **Figure 4**(**b**) shows well-distributed PLA-AuNPs. To affirm the synthesized PLA-AuNPs' chemical composition, EDX was employed to investigate the chemical composition of the as-produced PLA-AuNPs, as per **Figure 4**(**a**)**and 4**(**b**). The EDX spectrum confirmed that the as-produced PLA-AuNPs were composed of gold (Au) only, and displayed no other element except the peak corresponding to carbon (C) and oxygen (O). The presence of the C peak was due to the carbon electrode on to which the sample was drop cast.

The EDX spectrum also showed the presence of O indicating that oxygen was adsorbed on the carbon electrode because the film was exposed to air. This confirms that oxygen is adsorbed on carbon nanotubes if they are exposed to air for a long time[41]. Although there are various gas molecules in air, oxygen was believed to be the main adsorbate on the air-exposed carbon nanotubes[42], possibly due to its faster adsorption compared with other molecules[43]. This was based on finding that oxygen was the main adsorbate on the carbon electrode during overnight air exposure in sample preparation and reinforced the chemical purity of the PLA-AuNPs. The ratio of anodic and cathodic peak (i_{pa}/i_{pc}) was almost 1, which gave constant peak potential as the scan rate increased[44]. Moreover, the anodic and cathodic peak potentials were consistent at different scan rates[45] suggesting that the electrochemical reaction was reversible based on peak separation (**Figure 5**). The active surface area of the modified electrode was calculated using the Randles-Sevick equation ($i_{pc} = (2.69\times10^5)\, n^{3/2}\, AD^{1/2}\, Cv^{1/2}$). From the slope of the plot i_{pc} versus $v^{1/2}$ in **Figure 5**(**a**) and (**b**), the surface area of the electrodes was calculated as 0.26 cm^2 and 0.41 cm^2 for the bare SPCE and PLA-AuNPs, respectively. This result confirmed that the improvement afforded by PLA-AuNPs on the active surface area was relatively higher compared with bare SPCE. The derived result was comparable to that of polymer-embedded gold nanoparticles (β-CD-EDAS(N-[3-(trimethoxysilyl)propyl]ethylene-diamine matrix encapsulated gold nanoparticles), which revealed that a high active surface area enhanced the process of electron-transfer and therefore resulted in better sensitivity[46].

The modified SPCE electrochemical reaction was in a process of controlled diffusion, shown by a reduction in the $K_3[Fe(CN)_6]^{3-/4-}$ peak current, which in turn relied on the current of the scan rate square root ($v^{1/2}$). To get a better view of the modified electrode properties, an electrochemical impedance spectroscopy (EIS) study was performed to correlate with the performance of the modified electrode presented in terms of CV measurements. The semicircle section seen at high frequencies correlated with the limiting process of the electron transfer in the EIS. The charge transfer resistance (R_{ct}) was measured directly as the diameter of the semicircle. This result tallied with the value of R_{ct} of the bare SPCE, which was 1932 Ω and where the modification of SPCE/PLA-AuNPs decreased to 1444 Ω (**Figure 6**). The decrease of R_{ct} value in SPCE/PLA-AuNPs may have resulted from a decrease in local dielectric constant and/or an increase in the thickness of the electric double layer[47], suggesting that $K_3[Fe(CN)_6]^{3-/4-}$ function by adsorption at the metal/solution interface. These outputs complied with the ones derived from the measurements of CV (**Figure 7**). The peak currents increased progressively with the modification of the SPCEs using PLA-AuNPs, which showed that a higher sensitivity was the inverse of the lower R_{ct}[48]. Thus, the increase in the value of CV of the modified electrodes and the decrease in R_{ct} values may have been due to the gradual replacement of water molecules (the volume of the water molecules is 27.19 $Å^3$) by the adsorption of the $K_3[Fe(CN)_6]^{3-/4-}$ on the metal surface, decreasing the extent of the dissolution reaction[49].

Table 3 indicates the relative standard deviation (RSD) of the repeatability and reproducibility of the modified electrode. Routine CV recording of $K_3[Fe(CN)_6]^{3-/4-}$ was made for six consecutive sets to investigate the repeatability of the modified electrodes. The RSD of SPCE/PLA-AuNPs was derived as 4.26%. The electrode with PLA-AuNPs modification gave better RSD after several measurements. Moreover, using the same procedure, six modified electrodes were independently fabricated, which gave RSD values of 4.05% for SPCE/PLA-AuNPs, indicating better reproducibility of the electrode fabrication for PLA-AuNPs. The modified substrate depending on PLA-AuNPs was kept at 37 °C for an extended duration. It was also utilized for the record of 20 cycles and a decrease of 18% in signal quality. In order to achieve the maximum output from the biosensor, immobilization period, temperature, together with ssDNA concentration and criteria for hybridization were examined. These conditions needed to be optimized, as they influence the peak current of DPV. To optimize the ssDNA concentration, SPCE/PLA-AuNPs was pipetted with different concentration (0.2, 0.4, 0.6, 0.8, 1.0, 1.2 and 1.4 µM) of ssDNA for 60 min so that the optimum concentration of ssDNA was determined. Based on **Figure 8**, the DPV peak current increased as higher DNA concentrations were used. The study also found that the optimized concentration of the DNA was 1.2 µM ssDNA.

To optimize the immobilization period involving the single-stranded DNA in SPCE/PLA-AuNPs, 25 µL of ssDNA (1.2 µM) were tested over different times (30, 60, 90, 120, 150, 180 and 210 min). In **Figure 9**, the findings show an increase in immobilization period resulting in the continuous increase of the DPV peak current. Thus, the optimum immobilization time of the ssDNA was selected as 180 min. To optimize the immobilization temperature, the SPCE/PLA-AuNPs was pipetted with ssDNA (1.2 µM) in various temperatures (75, 65, 55, 45, 35, and 25 °C) for 180 min. We found that when the temperature of immobilization was increased to 55 °C, the DPV peak current initially escalated followed by a subsequent depreciation (**Figure 10**); thus, 55 °C was selected as the optimized immobilization temperature to be used in subsequent experiments. Separation of ssDNA that is immobile from surfaces of the electrode and hybridization disablement was caused by increased temperatures. There have been other reports with similar results[50]. Faster splitting and degeneration of DNA from the surfaces of nanoparticles of gold occurred at higher temperatures[51]. Research conducted recently reported that the bond between gold and thiol oxidizes degrades quickly and simply in a situation that is ambient, for example when exposed to water, air, and light[52,53,54]. The effect of hybridization time was also investigated in this study.

The fabricated SPCE/PLA-AuNPs/ssDNA was drop-cast with a solution of target DNA (0.2 µM) at different hybridization times (5, 10, 15, 20, 25, and 30 min). The response of the DPV rose obviously, with a 5-min increase in time of incubation (from 5 to 10 min) (**Figure 11**). Once this value was obtained, a 10 to 30 min downward pattern was observed so the desired time for hybridization was chosen as 10 min. The efficiency of hybridization increased with an increase in temperature from 25 °C to 35 °C (**Figure 12**). The high current was seen to slowly decrease at a temperature higher than 35 °C. The reason for this was attributed to sandwich structure denaturation reducing the detection signal. Hence, the optimal hybridization temperature selected was 35 °C. The process we used in detecting *V. parahaemolyticus* comprised AuNPs to enhance the active surface area of the working electrode, PLA to mediate the surface modification and the redox complex, MB, to reduced it to LB. The outcome of this oxidation process was a better affinity between ssDNA and MB[55]. The DPV current was decreased due to the lower number of attached MB molecules during hybridization of ssDNA with its complementary sequence.

We conducted further investigations into the performance of the developed biosensor. The DPV results in **Figure 13** show that it was able to selectively distinguish probe DNA, complementary DNA, one-base mismatched DNA, three-base mismatched DNA, and non-complementary DNA in the presence of MB as the detection label[56,57]. The lowest peak current (0.73 µA) was exhibited by complementary DNA, which slowly increased by one-base mismatched DNA (0.94 µA), three-bases mismatched DNA (1.05 µA), non-complementary DNA (3.25 µA), and probe DNA (4.79 µA). The target DNA current was the smallest of all the currents of oligonucleotide sequences allowing our biosensor to discriminate between the sequences of oligonucleotide sensitively and specifically. MB bound strongly with ssDNA of immobilized probe DNA producing a large DPV peak current. SPCE/PLA-AuNPs/non-complementary DNA reduced the immobilized probe DNA current by almost half as only a small amount of MB assembled on the surface of SPCE/PLA-AuNPs/dsDNA. This is likely to be due to inaccessible interactions between MB and guanine bases. The interaction modes of DNA and MB are strongly dependent on such experimental conditions as pH, temperature, DNA concentration, ionic strength, and type of buffer[58,59]. MB commonly links to dsDNA by groove and intercalative modes, resulting in MB accumulation on dsDNA surface[60]. The exposure of our capture probe DNA to one-base mismatched DNA and three-base mismatched DNA consistently reduced DPV peak currents and the complementary target DNA continued this trend. **Table 4** shows the percentage of selectivity rate for MB peak current. Our overall finding was that hybridization of the constructed DNA biosensor was highly selective via immobilized probe DNA on the SPCE/PLA-AuNPs' surface.

The sensitivity of the developed DNA biosensor was further investigated with various concentrations of complementary target oligonucleotide. **Figure 14** depicts the gradual depletion of DPV peak current of MB on the SPCE/PLA-AuNPs as the complementary DNA concentration increased. **Figure 15** exhibits a linear regression coefficient of 0.96 which was generated between the log of reduced MB peak current and the log of several concentration of target DNA (0.2 pM to 0.02 mM). A graph of the peak current changes (ΔP) was plotted using the 3σ/m formula (σ being the standard deviation of blank solution and m being the slope of the linear curve)[61,62,63]. The detection limit of the fabricated DNA biosensor was calculated to be 4.43 pM which was greater than our smallest actually measured sample. This outcome was in agreement with the fact that ΔP for 0.2 pM and 2 pM (2.65×10^{-6} A and 2.81×10^{-6} A) with a standard deviation of 1.19×10^{-7} A and 1.06×10^{-7} A, respectively, overlapped.

To compute the LOQ for the fabricated DNA biosensor, we used the 10σ/m formula in which (σ is the blank solution standard deviation and m is the slope of the linear curve) and found the outcome to be a gain of 14.8 pM. Repeated denaturation of the complementary DNA was performed to assess the DNA biosensor in terms of its regeneration capacity. We did this by incubating 0.2 µM complementary DNA-modified electrode in hot water at 86 °C for 8 min to denature the double-stranded DNA, followed by rapid cooling in an ice bath to maintain the denatured single-stranded DNA[64].

The hybridization activity was maintained at 91% of its initial response after 8 efforts of regeneration (n = 5, RSD = 4.05%). The DNA biosensor based on SAM method for DNA probe immobilization on to SPCE/PLA-AuNPs was highly stable, achieving a good response in detecting complementary DNA after repeated denaturation processes. The stability of our DNA biosensor regarding heat was further explored. To do this, we stored the PLA-AuNPs/SPCE/ssDNA electrode at temperatures of 4 °C, 25 °C, and 45 °C in a sealed aluminum pouch containing silica gels. At the end of 6 months, we assessed the complementary DNA and estimated the percentage of recovery of signal production. **Figure 16** shows that the probe SPCE/PLA-AuNPs/ssDNA was highly stable with more than 80% of its initial signal still recoverable after 6 months' storage. The strong reaction between PLA-AuNPs and ssDNA was found to have long-term stability at a temperature below 45 °C.

Nine different species of bacteria (*B. cereus*, *L. monocytogenes*, C. *jejuni*, *E. coli O157:H7*, *V. alginolyticus*, *S. typhimurium*, *S. enteritis*, *K. pneumonia* and *V. parahaemolyticus*) were screened by PCR detection. The PCR amplification products for species-specific detection of *V. parahaemolyticus* from the bacteria culture are shown in **Figure 17**. The toxR gene of *V. parahaemolyticus* was utilized as PCR primer for *V. parahaemolyticus* identification due to its presence in pathogenic isolates. From the PCR analysis, *V. parahaemolyticus* showed positive results due to the specificity of the PCR primer of the toxR gene towards *V. parahaemolyticus*. No PCR products from other bacterial strains were detected. The DPV peak current obtained after a cross-reactivity assessment showed very clear detection of *V. parahaemolyticus* in comparison with other bacteria species, as depicted in **Figure 18**. The DPV signal increased as the number of base pairs decreased, due to the larger amount of MB molecules bound to the probes. *V. parahaemolyticus* were clearly able to be discriminated from the other foodborne pathogens which mimicked the environment of the food sample.

Cockles were selected as real samples for the DNA biosensor validation in this study since they are popular ingredients in several types of local food. It is well known that raw cockles often carry pathogenic V. *parahaemolyticus* and can transmit these bacteria to humans, especially if they are inadequately refrigerated during storage after harvesting[65]. The treated group of cockle samples was stored at -20 °C for 24 h, and exposed to UV light at 20 °C for 4 h prior to DNA extraction during our pre-treatment step. **Figure 19** shows that the PCR analysis found *V. parahaemolyticus* in both the treated and untreated (spiked) samples. This is shown in Lane 7, 8, 9, 10, 11, and 12 correlating with the colony count in the previous discussion. No V. *parahaemolyticus* appears in the treated and untreated (unspiked) samples, as shown in Lane 1, 2, 3, 4, 5 and 6 in the PCR results although the colony count did indicate its presence in the samples. A possible reason for this is the presence of contaminating metabolites such as protein in the extracted DNA[66].

Figure 20 summarizes the detection results using the developed DNA biosensor, which successfully determined the presence of *V. parahaemolyticus* in the treated group consisting of spiked and unspiked samples. These results positively correlate with the previously discussed PCR results. Every sample of the PCR that showed positive results was discovered using the PLA-stabilized electrochemical biosensor technique, which is AuNP-based, and the DPV peak area clearly corresponded with the resulting PCR intensity bands (**Figure 19** and **Figure 20**). These results indicate that the suggested nanoparticle-based electrochemical sensor in this study detected *V. parahaemolyticus* successfully in the real samples, thus proving that it is superior to PCR with no effect on the authenticity of the results.

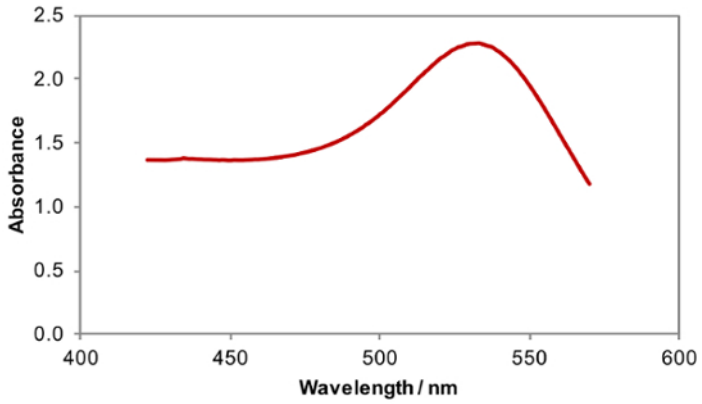

Figure 1: Absorbance of PLA-AuNPs Please click here to view a larger version of this figure.

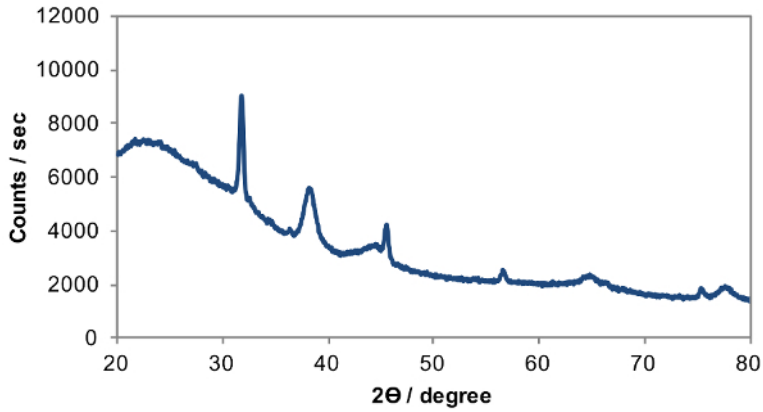

Figure 2: X-ray diffraction spectrum of PLA-AuNPs. Adapted with permission from ref. [30]. Copyright (2016) Sociedade Brasileira de Química. Please click here to view a larger version of this figure.

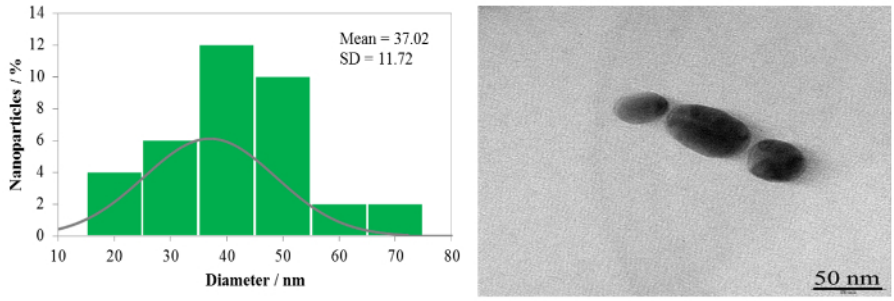

Figure 3: TEM frequency diameter distribution and images of PLA-AuNPs at a measurement scale of 50 nm. Reprinted with permission from ref. [30]. Copyright (2016) Sociedade Brasileira de Química. Please click here to view a larger version of this figure.

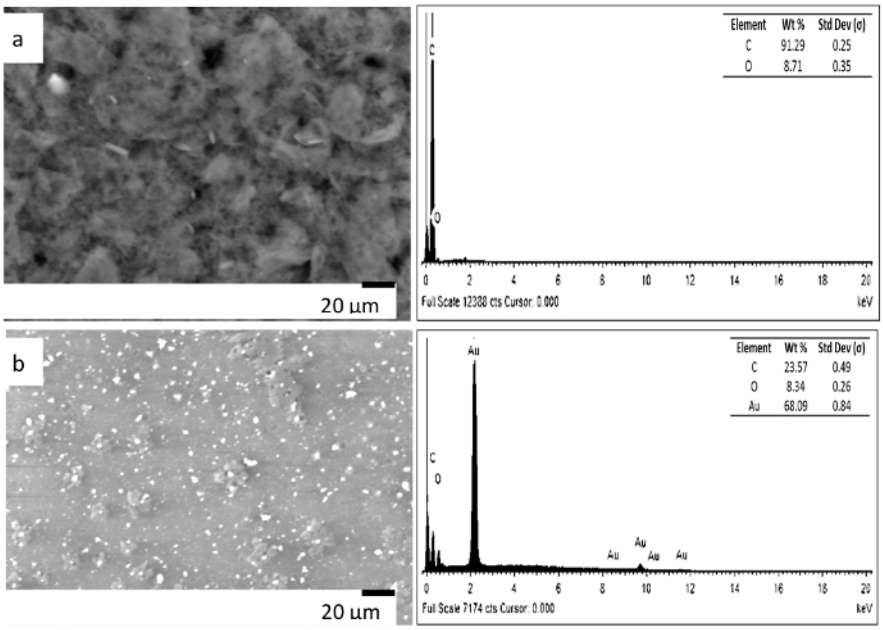

Figure 4: EDX spectra and FESEM images of (a) bare SPCE and (b) SPCE/PLA-AuNPs. Reprinted with permission from ref. [30]. Copyright (2016) Sociedade Brasileira de Química. Please click here to view a larger version of this figure.

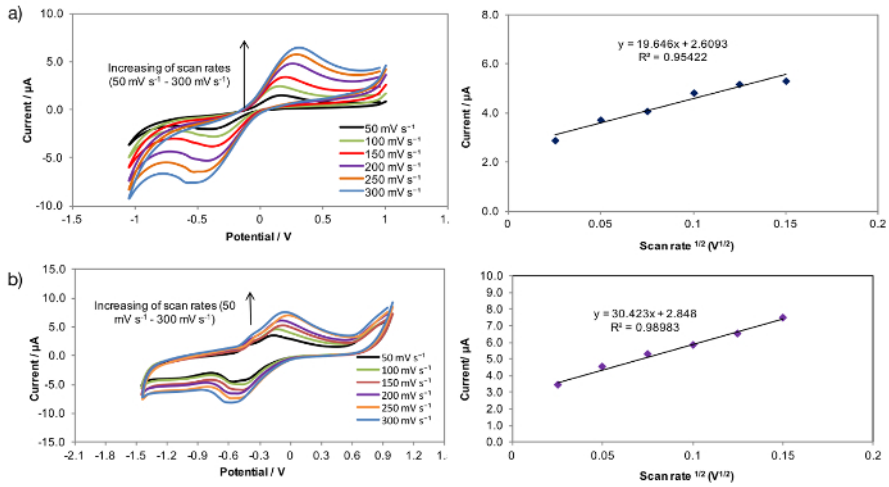

Figure 5: The plot of peak current oxidation against the scan rate square root and cyclic voltammograms: (a) bare SPCE and (b) SPCE/PLA-AuNPs in 1.0 mmol L^{-1} $K_3[Fe(CN)_6]$ (pH 7). The scan rates were 300, 250, 200, 150, 100, and 50 mV s^{-1}. Adapted with permission from ref. [30]. Copyright (2016) Sociedade Brasileira de Química. Please click here to view a larger version of this figure.

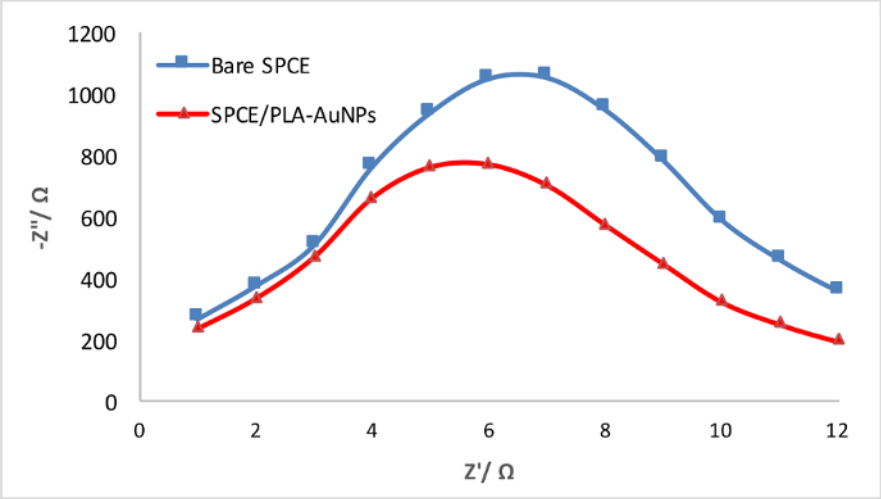

Figure 6: Impedance spectra of modified electrodes in 1.0 mmol L^{-1} $K_3[Fe(CN)_6]$ (pH 7). Amplitude: 5 mV, and frequency range: 0.1-10^5 Hz. Adapted with permission from ref. [22]. Copyright (2016) Elsevier. Please click here to view a larger version of this figure.

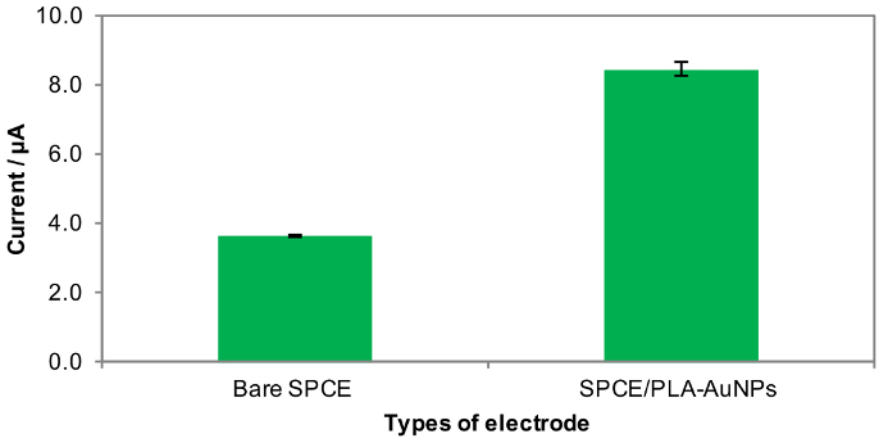

Figure 7: Anodic peak current of modified electrodes in 1.0 mmol L^{-1} $K_3[Fe(CN)_6]$ (pH 7) at a scan rate of 0.1 V s^{-1} using cyclic voltammetry measurement Please click here to view a larger version of this figure.

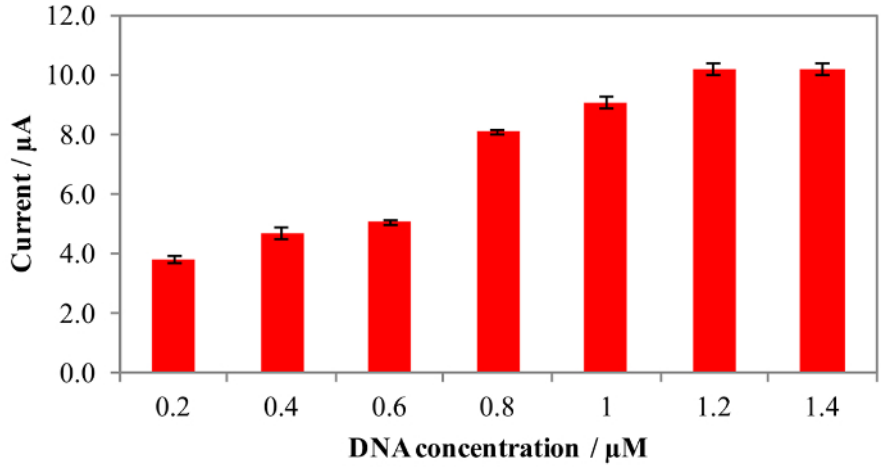

Figure 8: Effect of concentration for ssDNA immobilization on SPCE/PLA-AuNPs in 0.1 mol L^{-1} PBS (pH 7) at scan rates of 0.1 V s^{-1} after 30 min incubation in 20 µM MB using differential pulse voltammetry measurement Please click here to view a larger version of this figure.

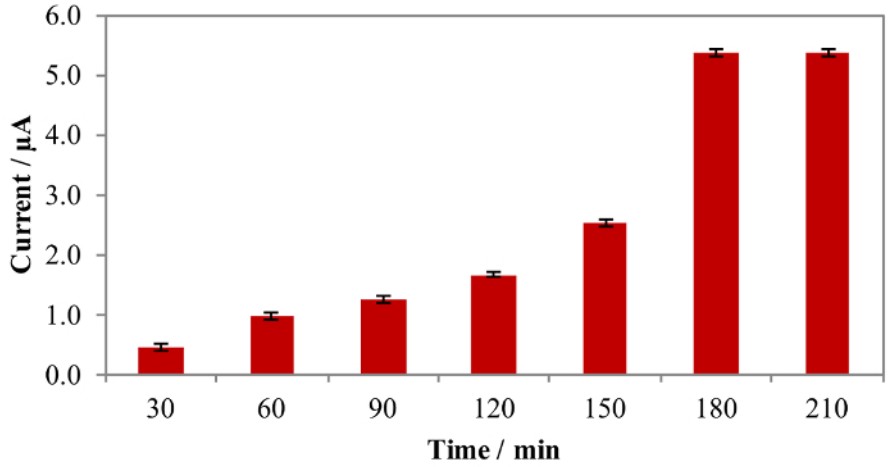

Figure 9: Effect of ssDNA immobilization time on SPCE/PLA-AuNPs in 0.1 mol L^{-1} PBS (pH 7) at a scan rate of 0.1 V s^{-1} after 30 min incubation in 20 µM MB using differential pulse voltammetry measurement Please click here to view a larger version of this figure.

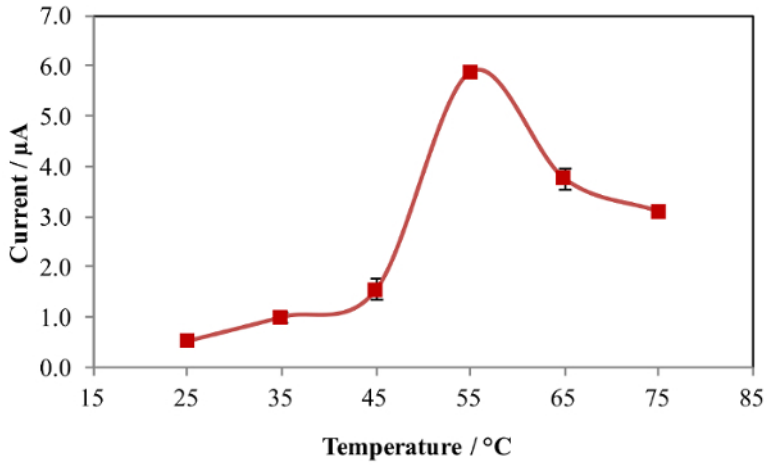

Figure 10: Effect of ssDNA immobilization temperature on SPCE/PLA-AuNPs at a scan rate of 0.1 V s^{-1} at 0.1 mol L^{-1} PBS (pH 7) after an incubation period of 30 min in 20 µM of MB using differential pulse voltammetry measurement Please click here to view a larger version of this figure.

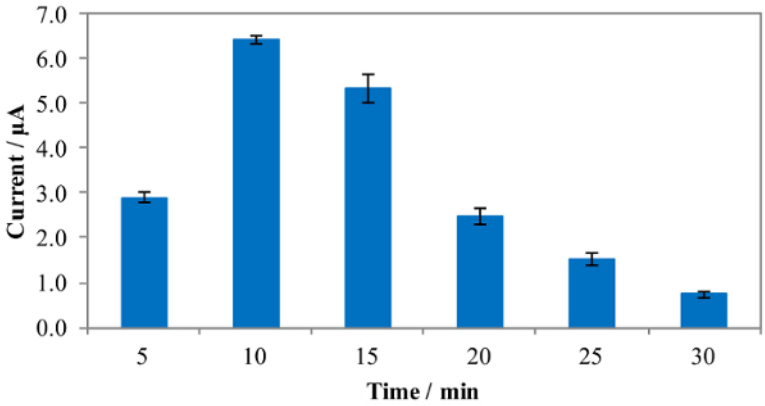

Figure 11: Effect of hybridization time on SPCE/PLA-AuNPs/ssDNA in 0.1 mol L^{-1} PBS (pH 7) at a scan rate of 0.1 V s^{-1} after 30 min incubation in 20 µM MB using differential pulse voltammetry measurement Please click here to view a larger version of this figure.

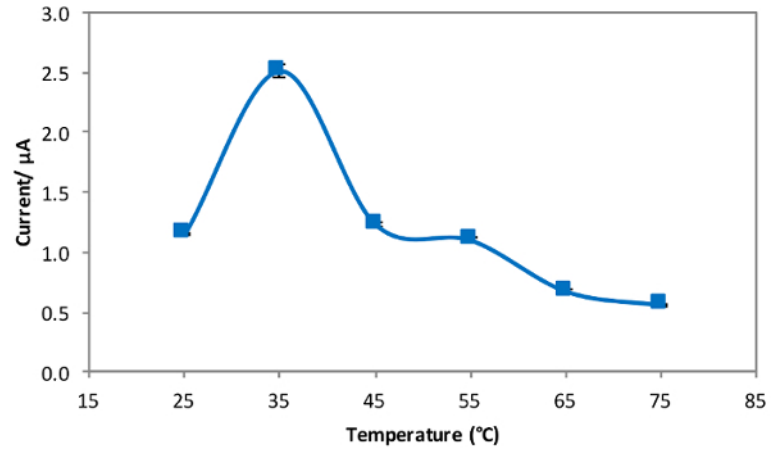

Figure 12: Effect of hybridization temperature on SPCE/PLA-AuNPs/ssDNA in 0.1 mol L^{-1} PBS (pH 7) at a scan rate of 0.1 V s^{-1} after 30 min incubation in 20 µM MB using differential pulse voltammetry measurement. Reprinted with permission from ref. [22]. Copyright (2016) Elsevier. Please click here to view a larger version of this figure.

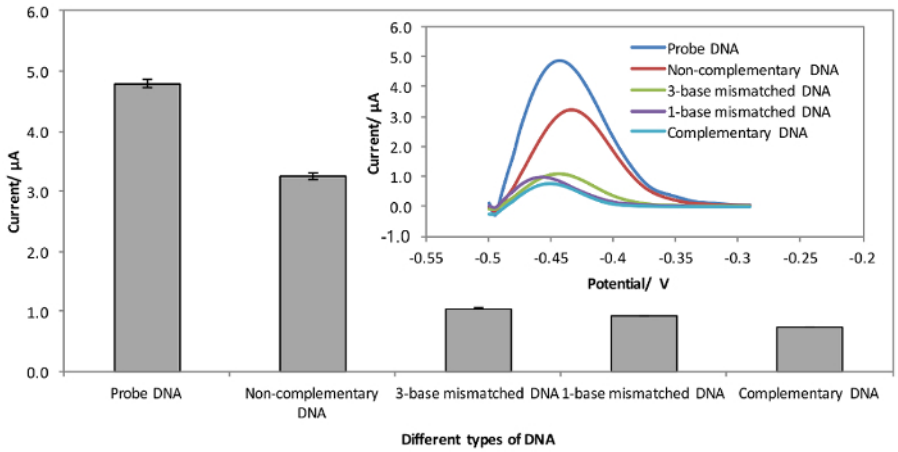

Figure 13: Histogram of the MB reduction peak current using different types of DNA in 0.1 mol L^{-1} PBS (pH 7) at a scan rate of 0.1 V s^{-1} after 30 min incubation in 20 µM MB. The inset illustrates differential pulse voltammograms in the same conditions. Reprinted with permission from ref. [22]. Copyright (2016) Elsevier. Please click here to view a larger version of this figure.

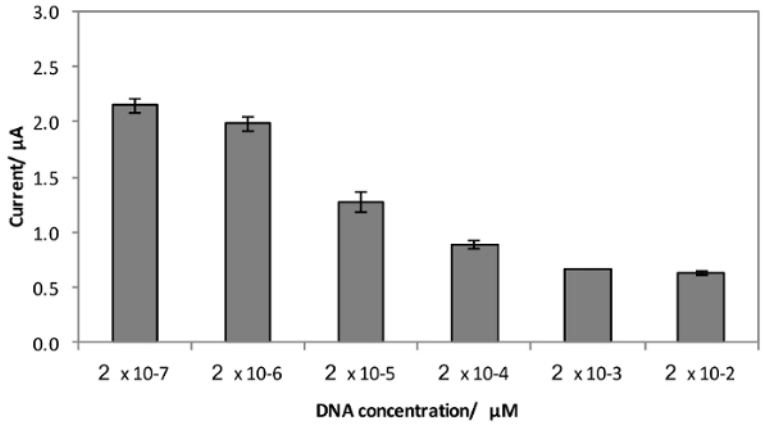

Figure 14: Histogram of the MB reduction peak current using different DNA concentration in 0.1 mol L^{-1} PBS (pH 7) at a scan rate of 0.1 V s^{-1} after 30 min incubation in 20 µM MB using differential pulse voltammetry measurement. Reprinted with permission from ref. [22]. Copyright (2016) Elsevier. Please click here to view a larger version of this figure.

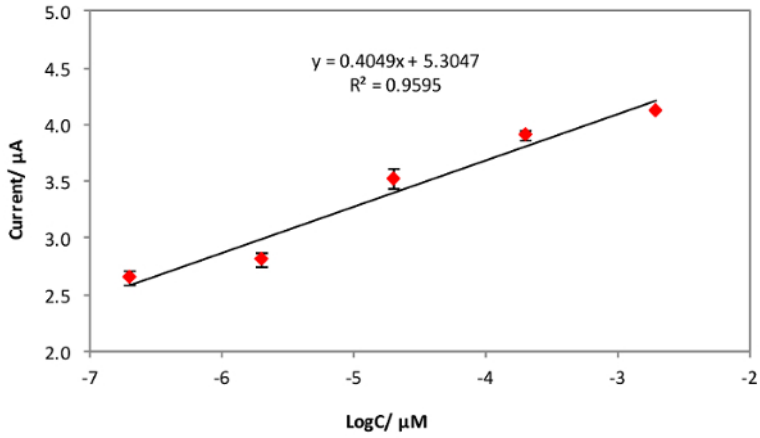

Figure 15: A linear plot of the reduction peak current of MB against the log of different DNA concentration in 0.1 mol L^{-1} PBS (pH 7) at a scan rate of 0.1 V s^{-1} after 30 min incubation in 20 µM MB using differential pulse voltammetry measurement. Reprinted with permission from ref. [22]. Copyright (2016) Elsevier. Please click here to view a larger version of this figure.

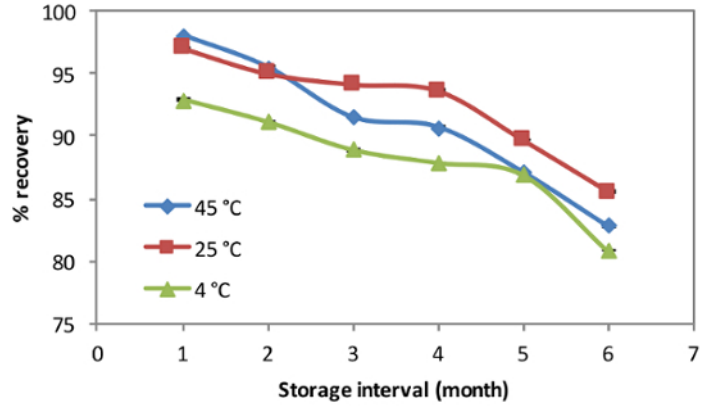

Figure 16: Effect of different hybridization temperatures on SPCE/PLA-AuNPs/ssDNA at 6 months of storage interval (*n* = 3). Measurements were made in 0.1 mol L^{-1} PBS (pH 7) at a scan rate of 0.1 V s^{-1} after 30 min incubation in 20 µM MB using differential pulse voltammetry measurement. Reprinted with permission from ref. [22]. Copyright (2016) Elsevier. Please click here to view a larger version of this figure.

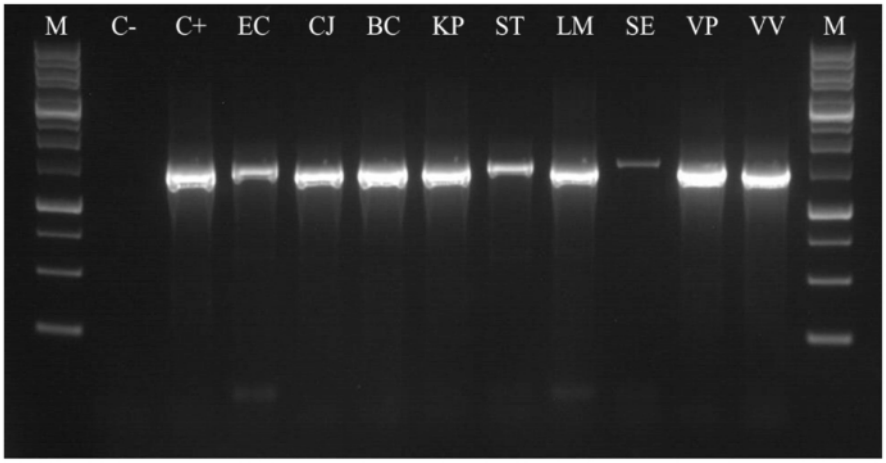

Figure 17: Agarose gel electrophoresis-PCR amplification using 16S rRNA gene sequencing products of selected bacteria from bacteria culture. Lane M: 1kb DNA ladder, Lane C−: negative control (sterile distilled water), Lane C+: positive control (DNA extracted from *E. coli* is used as template), Lane EC: *E. coli* O157:H7, Lane CJ: *C. jejuni*, Lane BC: *B. cereus*, Lane KP: *K. pneumonia*, Lane ST: *S. typhimurium*, Lane LM: *L. monocytogenes*, Lane SE: *S. enteritis*, Lane VP: *V. parahaemolyticus* and Lane VV: *V. alginolyticus* Please click here to view a larger version of this figure.

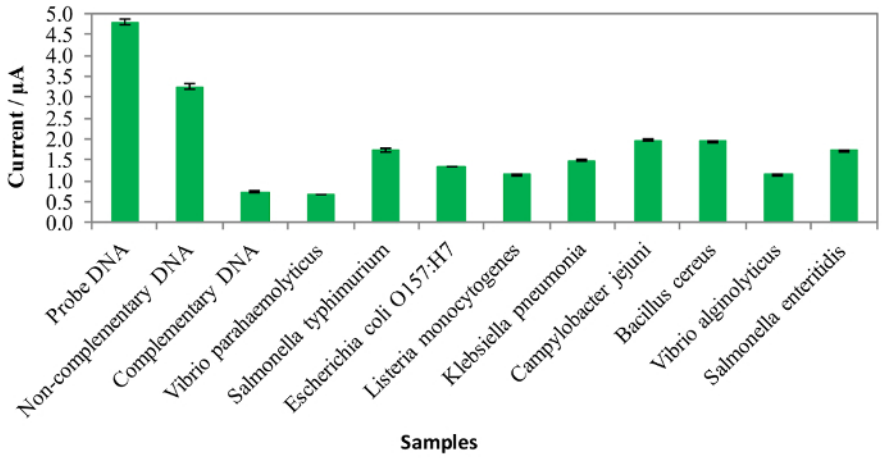

Figure 18: Histogram of the MB reduction peak current for cross-reactivity study of the DNA biosensor against various foodborne pathogens in 0.1 mol L^{-1} PBS (pH 7) at a scan rate of 0.1 V s^{-1} after 30 min incubation in 20 µM MB using differential pulse voltammetry measurement. Reprinted with permission from ref. [23]. Copyright (2017) Springer. Please click here to view a larger version of this figure.

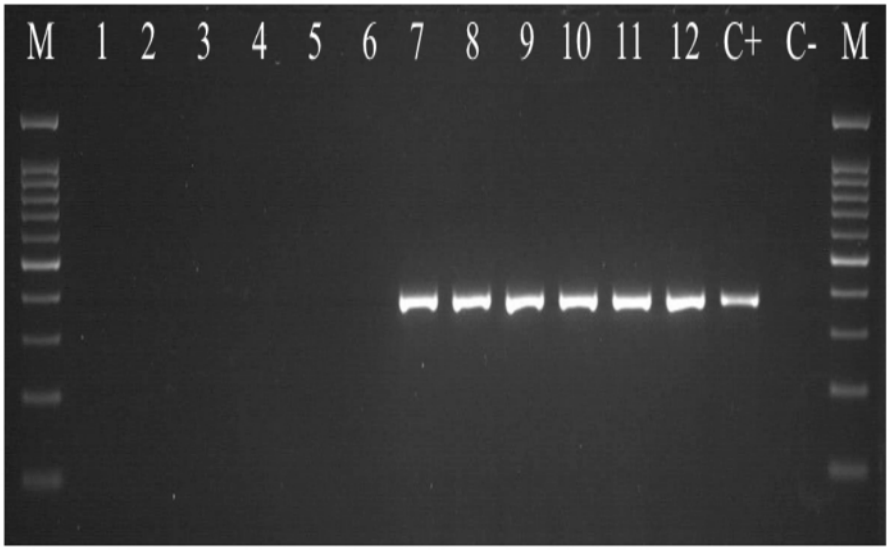

Figure 19: Agarose gel electrophoresis-PCR amplification products of *V. parahaemolyticus* from fresh cockle samples. Lane M: 2ul of 100 bp DNA ladder, Lane 1-3: untreated unspiked samples, Lane 4-6: treated unspiked samples, Lane 7-9: untreated spiked samples, Lane 10-12: treated spiked samples, Lane C+: positive control (*V. parahaemolyticus* ATCC 17802), Lane C-: negative control (sterile distilled water). Reprinted with permission from ref. [23]. Copyright (2017) Springer. Please click here to view a larger version of this figure.

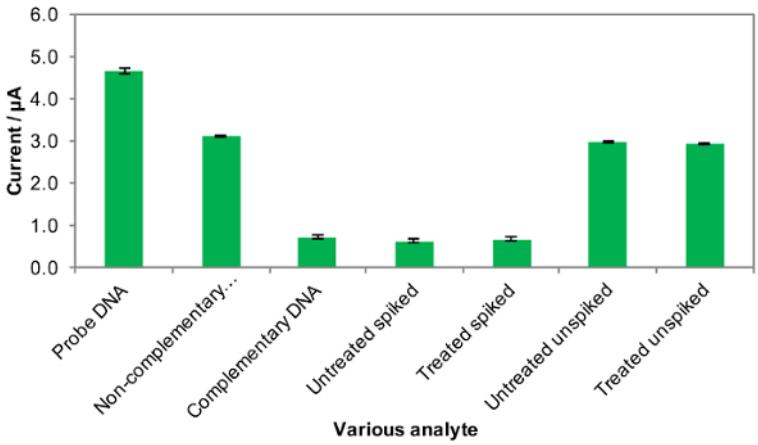

Figure 20: Histogram of the MB reduction peak current for detection of *V. parahaemolyticus* in fresh cockle samples using the DNA biosensor in 0.1 mol L^{-1} PBS (pH 7) at a scan rate of 0.1 V s^{-1} after 30 min incubation in 20 µM MB using differential pulse voltammetry measurement. Reprinted with permission from ref. [23]. Copyright (2017) Springer. Please click here to view a larger version of this figure.

Electrode composition	Incubation time (h)	Temperature (°C)	Growth media
Campylobacter jejuni	48	42	BA/ BB
Listeria monocytogenes	48	30	TSA/ TSB
Salmonella typhimurium	24	37	TSA/ TSB
Salmonella enteritidis	24	37	TSA/ TSB
Klebsiella pneumonia	24	37	EMBA/ TSB
Escherichia coli O157:H7	24	37	MA/ TSB
Bacillus cereus	24	37	MYPA/ TSB
Vibrio alginolyticus	24	37	TSA+3% NaCl/TSB+3% NaCl
Vibrio parahaemolyticus	24	37	CA/TSA+3% NaCl/TSB+3% NaCl

Table 1: Culture conditions of selected bacteria.

Sample	Pos. [°2Th.]	FWHM [°2Th.]	d-spacing [Å]	Crystallite size (nm)
PLA-AuNPs	31.682	0.3149	2.8243	27

Table 2: The size of the PLA-AuNP crystallites. Adapted with permission from ref. [30]. Copyright (2016) Sociedade Brasileira de Química.

Modified electrode	% RSD (n = 6)		Signal reduction (%) (n = 20)	
	Repeatability	Reproducibility		
SPCE/PLA-AuNPs	4.26	4.05	18	

Table 3: Properties of modified electrodes relating to AuNPs and PLA-AuNPs modification in $K_3[Fe(CN)_6]$ with 1.0 mmol L^{-1} concentration at a scan rate of 0.1 V s^{-1}. Adapted with permission from ref. [30]. Copyright (2016) Sociedade Brasileira de Química.

Electrode composition	i_{pa} **(μA)** (n = 3)	E_{pa} **(V)**	**Selectivity rate (%)**
SPCE/PLA-AuNP/probe DNA	4.79 ± 0.10	-0.46	-
SPCE/PLA-AuNP/non-complementary DNA	3.25 ± 0.12	-0.44	67.85
SPCE/PLA-AuNP/3-bases mismatched DNA	1.05 ± 0.11	-0.45	21.92
SPCE/PLA-AuNP/1-base mismatched DNA	0.94 ± 0.12	-0.46	19.62
SPCE/PLA-AuNP/complementary DNA	0.73 ± 0.10	-0.45	15.24

Table 4: DPV selectivity of MB peak current in 0.1 mol L^{-1} PBS (pH 7) at a scan rate of 0.1 V s^{-1} after 30 min incubation in 20 μM MB

Composition of the electrodes	Detection method	Linear range (M)	Detection limit (M)	References
3D AuNPs	DPV	1.5×10^{-6} - 7.0×10^{-9}	2.0×10^{-10}	69
(+)AuNPs	DPV	1.0×10^{-9} - 1.5×10^{-12}	2.6×10^{-12}	70
AuNPs/GR	DPV	1.3×10^{-9} - 2.5×10^{-11}	8.3×10^{-12}	71
AuNPs-ADH-GSs	DPV	5.0×10^{-8} - 3.0×10^{-13}	3.0×10^{-13}	72
AuNPs-MPTS	DPV	5.0×10^{-9} - 1.0×10^{-11}	5.0×10^{-11}	73
AuNPs–GO	DPV	1.0×10^{-9} - 1.0×10^{-14}	3.5×10^{-15}	74
CoS/AuNPs	DPV	1.0×10^{-9} - 1.0×10^{-12}	7.0×10^{-13}	75
PLA-AuNPs	DPV	2.0×10^{-8} - 2.0×10^{-13}	5.3×10^{-12}	This work

Table 5: Comparison of some of the recently developed electrochemical DNA nanosensors. Reprinted with permission from ref. [22]. Copyright (2016) Elsevier.

Discussion

The critical steps in a framework for successful development of this type of electrochemical biosensor are selection of appropriate biological recognition elements for the transducer (nucleic acid or DNA here); chemical approach for constructing the sensing layer of the transducer; transduction material; optimization of DNA immobilization and hybridization; and validation of the developed biosensor using real samples.

Core to the successful development of a sensitive and selective electrochemical DNA biosensor, is the optimization of the immobilization and hybridization condition. In this work, we used MB as the redox complex. There are various principles of MB-DNA interactions: (i) by electrostatic interaction of the MB cationic charge with the phosphate backbone anionic charge of both ssDNA and dsDNA; (ii) by MB intercalation through successful insertion of MB between alternating G-C base pairs in dsDNA; (iii) by covalent bond to the end of the target ssDNA, which produces a low label density (one or two MB molecules per DNA strand); and (iv) by MB interactions with an unbound guanine base in ssDNA. We applied the fourth principle, which accurately identifies *V. parahaemolyticus* from cross reactivity of bacteria and in fresh cockles. After oxidization of particular interest, there was a stronger affinity between MB and ssDNA. Hybridization of ssDNA with its complementary sequence replaces the bonded MB molecules, and thus reduces the signal.

The series of experimental results presented above focuses on the development of a rapid method of detecting *V. parahaemolyticus* with high selectivity and sensitivity using the principles of DNA hybridization. The first step is the synthesis and characterization of polylactic acid-stabilized

gold nanoparticles (PLA-AuNPs) for modification of the electrode (**Figures 1-6** and **Table 2**). The quality of the gold nanoparticles was evaluated using Ultraviolet-visible Spectroscopy (UV-Vis), X-ray Diffraction (XRD), Field-emission Scanning Electron Microscopy (FESEM), Transmission Electron Microscopy (TEM), Cyclic Voltammetry (CV) and Impedance analysis. The second part of the development involved an electrochemical characterization of the modified electrode (**Figures 7-12** and **Table 3-4**) which determined the successful enhancement of the modified electrode relative to the bare electrode in terms of detecting the hybridization event.

The third step of the DNA based biosensor development was based on the optimization of the experimental conditions of the hybridization event and the application of the developed biosensor to the detection of the actual pathogen (**Figures 13-20**). The hybridization event which determined the success of the detection of the pathogen was assessed using differential pulse voltammetry (DPV). The positive existence of the targeted pathogen was indicated through reduction of the current. The sensitivity of the developed biosensor was evaluated through the construction of a calibration plot and the calculation of LOD (**Figure 15**). The fabricated biosensor was able to specifically distinguish *V. parahaemolyticus* from other pathogens based on the different levels of current reduction (**Figures 17 and 18**). The evaluation of the feasibility of the developed biosensor for detection of *V. parahaemolyticus* in actual food sample is presented in **Figures 19 and 20** and the positive existence of the targeted pathogen is indicated by reduction of the current. The successful development of DNA-based biosensors is highly dependent on DNA probe selection, enhancement of the modified electrode as well as the optimization of the experimental conditions. The DNA probe here has been adapted from the previous work of Nakano[67]. Enhancement of the modified electrodes was performed by using gold nanoparticles stabilized with polylactic acid to enable the standardization of the nanosize. The gold nanoparticles function as electro catalytic material[68] and act to increase the transfer rate of the electron and also provide a surface on which to anchor the DNA probe. The experimental parameters were optimized in terms of temperature and incubation time which is crucial for DNA to form duplex. The hybridization temperature affects the separation between the non-specific adsorption and this increases the selectivity of the sensor. Incubation time of the hybridization increases the chances of the duplex formation. The immobilization procedure must be optimized in order to make sure the DNA probe will be in suitable orientation for the duplex formation to form.

Table 5 compares a sample of recently developed electrochemical DNA biosensors[69,70,71,72,73,74,75,]. DNA-based biosensing is a promising method for replacing molecular based techniques although there are a few limitations that must be addressed before the method can be portable enough for onsite usage. The main limitation is sample processing DNA extraction as the purity and the amount of DNA extracted on site is not likely to be as good as that extracted by the standard lab-based method. It is, however, a promising alternative if the PCR and gel electrophoresis can be replaced with sample pretreatment system such as microfluidic.

DNA-based biosensors are potentially useful for many applications including medical diagnostics, environmental monitoring and food monitoring. This technique will enable online monitoring of quality control processes as well as point-of-care monitoring of patients. The portability of the whole sensor system will enable the decentralization of diagnostic processes where the consumer can use the detection system in the comfort of their home.

Disclosures

The authors have nothing to disclose.

Acknowledgements

The authors would like to acknowledge the support of Universiti Putra Malaysia.

References

1. Gould, L. H., Rosenblum, I., Nicholas, D., Phan, Q., and Jones, T. F. Contributing factors in restaurant-associated foodborne disease outbreaks, FoodNet sites, 2006 and 2007. *Journal of Food Protection.* **76** 1824-1828 (2013).
2. Arvanitoyannis, I. S., Kotsanopoulos, K. V., and Papadopoulou, A. Rapid detection of chemical hazards (toxins, dioxins, and PCBs) in seafood. *Critical Reviews in Food Science and Nutrition.* **54** 1473-1528 (2014).
3. Robertson, L. J., Sprong, H., Ortega, Y. R., van der Giessen, J. W. B., and Fayer, R. Impacts of globalisation on foodborne parasites. *Trends in Parasitology.* **30** 37-52 (2014).
4. Sandilands, E. A., and Bateman, D. N. The epidemiology of poisoning. *Medicine.* **44** 76-79 (2016).
5. Boschi-Pinto, C., Velebit, L., and Shibuya, K. Estimating child mortality due to diarrhoea in developing countries. *Bulletin of the World Health Organization.* **86** 710-717 (2008).
6. Farthing, M. J. G. Diarrhoea: A Significant Worldwide Problem. *International Journal of Antimicrobial Agents.* **14** 65-69 (2000).
7. World Health Organization. *WHO estimates of the global burden of foodborne diseases: foodborne disease burden epidemiology reference group 2007-2015.* 1-255 (2015).
8. Yeung, M., and Boor, K. Epidemiology, pathogenesis, and prevention of foodborne Vibrio parahaemolyticus infections. *Foodborne Pathogens and Disease.* **1** 74-88 (2004).
9. Sakazaki, R. in *Foodborne Diseases.* eds D O Cliver & H P Riemann) 127-136 Academic Press, (2002).
10. Grochowsky, J., Odom, S. R., Akuthota, P., and Stead, W. Primary Septicemia and Abdominal Compartment Syndrome From Vibrio parahaemolyticus Infection in a 40-Year-Old Patient With No Known Immunocompromise. *Infectious Disease in Clinical Practice.* **22** 1 (2013).
11. Raghunath, P. Roles of thermostable direct hemolysin (TDH) and TDH-related hemolysin (TRH) in Vibrio parahaemolyticus. *Frontiers in Microbiology.* **5** 805 (2014).
12. Kalburge, S. S., Whitaker, W. B., and Boyd, E. F. High-Salt Preadaptation of Vibrio parahaemolyticus Enhances Survival in Response to Lethal Environmental Stresses. *Journal of Food Protection.* **77** 246-253 (2014).

13. Esteves, K., Hervio-Heath, D., Mosser, T., Rodier, C., Tournoud, M. G., Jumas-Bilak, E., Colwell, R. R., and Monfort, P. Rapid proliferation of Vibrio parahaemolyticus, Vibrio vulnificus, and Vibrio cholerae during freshwater flash floods in French Mediterranean Coastal lagoons. *Applied and Environmental Microbiology.* **81** 7600-7609 (2015).
14. Khandeparker, L., Anil, A. C., Naik, S. D., and Gaonkar, C. C. Daily variations in pathogenic bacterial populations in a monsoon influenced tropical environment. *Marine Pollution Bulletin.* **96** 337-343 (2015).
15. Caburlotto, G., Suffredini, E., Toson, M., Fasolato, L., Antonetti, P., Zambon, M., and Manfrin, A. Occurrence and molecular characterization of Vibrio parahaemolyticus in crustaceans commercialised in Venice area, Italy. *International Journal of Food Microbiology.* **220** 39-49 (2016).
16. Wong, H. C., Chen, M.-C., Liu, S.-H., and Liu, D.-P. Incidence of highly genetically diversified Vibrio parahaemolyticus in seafood imported from Asian countries. *International Journal of Food Microbiology.* **52** 181-188 (1999).
17. Rosec, J. P., Causse, V., Cruz, B., Rauzier, J., and Carnat, L. The international standard ISO/TS 21872-1 to study the occurence of total and pathogenic Vibrio parahaemolyticus and Vibrio cholerae in seafood: ITS improvement by use of a chromogenic medium and PCR. *International Journal of Food Microbiology.* **157** 189-194 (2012).
18. Maniyankode, R. A., Kingston, J. J., Murali, H. S., and Batra, H. V. Specific identification of vibrio parahaemolyticus employing monoclonal antibody based immunoassay. *International Journal of Pharmacy and Biological Sciences.* **4** (2), B156-B164 (2013).
19. Suffredini, E., Lopez-Joven, C., Maddalena, L., Croci, L., and Roque, A. Pulsed-field gel electrophoresis and PCR characterization of environmental Vibrio parahaemolyticus strains of different origins. *Applied and Environmental Microbiology.* **77** 6301-6304 (2011).
20. Bhattacharyya, N., and Hou, A. A pentaplex PCR assay for detection and characterization of Vibrio vulnificus and Vibrio parahaemolyticus isolates. *Letters in Applied Microbiology.* **57** 233-240 (2013).
21. da Silva, E. T. S. G. *et al.* Electrochemical Biosensors in Point-of-Care Devices: Recent Advances and Future Trends. *ChemElectroChem.* **4** (4), 778-794 (2017).
22. Nordin, N., Yusof, N. A., Abdullah, J., Radu, S., and Hushiarian, R. Sensitive detection of multiple pathogens using a single DNA probe. *Biosensors and Bioelectronics.* **86** 398-405 (2016).
23. Nordin, N., Yusof, N. A., Abdullah, J., Radu, S., and Hushiarian, R. A simple, portable, electrochemical biosensor to screen shellfish for Vibrio parahaemolyticus. *AMB Express.* **7** (1), 41 (2017).
24. Zhang, J., Li, Z., Zhang, H., Wang, J., Liu, Y., and Chen, G.. Rapid detection of several foodborne pathogens by F0F1-ATPase molecular motor biosensor. *Journal of Microbiological Methods.* **93** 37-41 (2013).
25. Barsan, M. M., Ghica, E. M., and Brett, C. M. A. in *Portable biosensing of food toxicants and environmental pollutants.* (eds D P Nikolelis, T Varzakas, A Erdem, & G-P Nikoleli) 33-69 CRC Press, Taylor & Francis Group, Boca Raton, (2014).
26. Kwun, J., Yun, S., Park, L., and Lee, J. H. Development of 1,1'-oxalyldiimidazole chemiluminescent biosensor using the combination of graphene oxide and hairpin aptamer and its application. *Talanta.* **119** 262-267 (2014).
27. Thavanathan, J., Huang, N. M., and Thong, K. L. Colorimetric biosensing of targeted gene sequence using dual nanoparticle platforms. *International Journal of Nanomedicine.* **10** 2711-2722 (2015).
28. Hushiarian, R., Yusof, N. A., Abdullah, A. H., Ahmad, S. A. A., and Dutse, S. W. Facilitating the indirect detection of genomic DNA in an electrochemical DNA biosensor using magnetic nanoparticles and DNA ligase. *Analytical Chemistry Research.* **6** 17-25 (2015).
29. Dutse, S. W., Yusof, N. A., Ahmad, H., Hussein, M. Z., Zainal, Z., Hushiarian, R., and Hajian, R.. An Electrochemical Biosensor for the Determination of Ganoderma boninense Pathogen Based on a Novel Modified Gold Nanocomposite Film Electrode. *Analytical Letters.* **47** (5), 819-832 (2014).
30. Nordin, N., Yusof, N. A., Abdullah, J., Radu, S., and Hajian, R. Characterization of Polylactide-Stabilized Gold Nanoparticles and Its Application in the Fabrication of Electrochemical DNA Biosensors. *Journal of the Brazilian Chemical Society.* **27** (9), 1679-1686 (2016).
31. Vongkamjan, K., Wang, S., and Moreno Switt, A.I. in *Rapid detection of foodborne bacterial pathogens in seafood.* Handbook of Seafood: Quality and Safety Maintenance and Applications, 247-257 (2016).
32. Wang, F., Jiang, L., Yang, Q., Han, F., Chen, S., Pu, S., Vance, A., and Ge, B. Prevalence and antimicrobial susceptibility of major foodborne pathogens in imported seafood. *Journal of Food Protection.*, **74** (9), 1451-1461 (2011).
33. Szermer-Olearnik, B., Sochocka, M., Zwolinska, K., Ciekot, J., Czarny, A., Szydzik, J., Kowalski, K., and Boratynski, J. Comparison of microbiological and physicochemical methods for enumeration of microorganisms. *Postepy Higieny i Medycyny Doswiadczalnej.*, **68** 1392-1396 (2014).
34. Ivanov, I. G., and Bachvarov, D. R. Determination of plasmid copy number by the "boiling" method. *Analytical Biochemistry.* **165** (1), 137-141 (1987).
35. Gopireddy, V.R. Biochemical tests for the identification of bacteria. *International Journal of Pharmacy and Technology.* **3** (4), 1536-1555 (2011).
36. Böhme, K., Fernández-No, I.C., Pazos, M., Gallardo, J.M., Barros-Velázquez, J., Cañas, B., and Calo-Mata, P. Identification and classification of seafood-borne pathogenic and spoilage bacteria: 16S rRNA sequencing versus MALDI-TOF MS fingerprinting. *Electrophoresis.* **34** (6), 877-887 (2013).
37. Seoudi, R., Fouda, A. A., and Elmenshawy, D. A. Synthesis, characterization and vibrational spectroscopic studies of different particle size of gold nanoparticle capped with polyvinylpyrrolidone. *Physica B: Condensed Matter.* **405** 906-911 (2010).
38. Mishra, A., Harper, S., and Yun, S. I. Interaction of biosynthesized gold nanoparticles with genomic DNA isolated from E. coli and S. aureus. *Nanotechnology (IEEE-NANO).* 1745-1750 (2011).
39. Sugimoto, T. Formation of modoispersed nano- and micro-particles controlled in size, shape, and internal structure. *Chemical Engineering and Technology.* **26** 313-321 (2003).
40. Rath, C., Sahu, K. K., Kulkarni, S. D., Anand, S., Date, S. K., Das, R. P., and Mishra, N. C. Microstructure-dependent coercivity in monodispersed hematite particles. *Applied Physics Letters.* **75** 4171-4173 (1999).
41. Abbas, M., Wu, Z.Y., Zhong, J., Ibrahim, K., Fiori, A., Orlanducci, S., Sessa, V., Terranova, M.L., and Davoli, I. X-ray absorption and photoelectron spectroscopy studies on graphite and single-walled carbon nanotubes: Oxygen effect. *Applied Physics Letters.* **87** (5), 051923 (2005).
42. Lim, S. C., Choi, Y.C., Jeong, H.J., Shin, Y.M., An, K.H., Bae, D.J., Lee, Y.H., Lee, N.S., and Kim, J.M. Effect of gas exposure on field emission properties of carbon nanotubes arrays. *Advanced Materials.* **13** 1563-1567 (2001).
43. Kim, B. H., Kim, B.R., and Seo, Y.G. A study on adsorption equilibrium for oxygen and nitrogen into carbon nanotubes. *Adsorption.* **11** 207-212 (2005).
44. Bard, A. J., and Faulkner, L.R. *Electrochemical methods: Fundamentals and applications.* John Wiley & Sons Inc., (2000).

45. Tan, Q., Wang, L., Ma, L., Yu, H., Ding, J., Liu, Q., Xiao, A., and Ren, G. Study on anion electrochemical recognition based on a novel ferrocenyl compound with multiple binding sites. *Journal of Physical Chemistry B.* **112** 11171-11176 (2008).
46. Manivannan, S., Ramaraj, R. Polymer-embedded gold and gold/silver nanoparticle-modified electrodes and their applications in catalysis and sensors. *Pure and Applied Chemistry.* **83** 2041-2053 (2011).
47. Benali, O., Larabi, L., Traisnel, M., Gengembre, L., and Hareka, Y. Electrochemical, theoretical and XPS studies of 2-mercapto-1-methylimidazole adsorption on carbon steel in 1 M HClO4. *Applied Surface Science.* **253** 6130-6139 (2007).
48. Shi, Y., Wen, L., Li, F., Cheng, H. M. Nanosized Li4Ti5O12/graphene hybrid materials with low polarization for high rate lithium ion batteries. *Journal of Power Sources.* **196** 8610-8617 (2011).
49. Bentiss, F., Traisnel, M., and Lagrenee, M. The substituted 1,3,4-oxadiazoles: a new class of corrosion inhibitors of mild steel in acidic media. *Corrosion Science.* **42** 127-146 (2000).
50. Wang, M., Gong, W., Meng, Q., and Zhang, Y. Electrochemical DNA impedance biosensor for the detection of DNA hybridization with polymeric film, single walled carbon nanotubes modified glassy carbon electrode. *Russian Journal of Electrochemistry.* **47** 1368-1373 (2011).
51. Herdt, A. R., Drawz, S. M., Kang, Y., Taton, T. A. DNA dissociation and degradation at gold nanoparticle surfaces. *Colloids and Surfaces B: Biointerfaces.* **51** (2), 130-139 (2006).
52. Bhatt, N., Huang, P. J. J., Dave, N., and Liu, J. Dissociation and degradation of thiol-modified DNA on gold nanoparticles in aqueous and organic solvents. *Langmuir.* **27** 6132-6137 (2011).
53. Liu, X., Jang, C.-H., Zheng, F., Jürgensen, A., Denlinger, J.D., Dickson, K.A., Raines, R.T., Abbott, N.L., and Himpsel, F.J. Characterization of protein immobilisation at silver surfaces by near edge X-ray absorption fine structure spectroscopy. *Langmuir.* **22** 7719-7725 (2006).
54. Willey, T. M., Andrew, L., Vance, T., Buuren, V., Bostedt, C., Terminello, L. J., and Fadley, C. S.. Rapid degradation of alkanethiol-based self-assembled monolayers on gold in ambient laboratory conditions. *Surface Science.* **576** (1), 188-196 (2005).
55. Farjami, E., Clima, L., Gothelf, K. and Ferapontova, E. E. DNA interactions with a Methylene Blue redox indicator depend on the DNA length and are sequence specific. *Analyst.* **135** 1443-1448 (2010).
56. Lin, X., Ni, Y. and Kokot, S. An electrochemical DNA-sensor developed with the use of methylene blue as a redox indicator for the detection of DNA damage induced by endocrine-disrupting compounds. *Analytica Chimica Acta.* **867** 29-37 (2015).
57. Zhang, F. T., Nie, J., Zhang, D. W., Chen, J. T., Zhou, Y. L., and Zhang, X. X. Methylene Blue as a G-Quadruplex Binding Probe for Label-Free Homogeneous Electrochemical Biosensing. *Analytical Chemistry.* **86** 9489-9495 (2014).
58. Ning, L., Li, X., Yang, D., Miao, P., Ye, Z., and Li, G. Measurement of Intracellular pH Changes Based on DNA-Templated Capsid Protein Nanotubes. *Analytical Chemistry.* **86** 8042-8047 (2014).
59. Sani, N. D. M., Heng, L. Y., Surif, S. and Lazim, A. M. in *AIP Conference Proceedings* Vol. 1571 (eds A. M. H. Abdul Murad *et al.*) 636-640 (2013).
60. Xu, P., Wang, J., Xu, Y., Chu, H., Shen, H., Zhang, D., Zhao, M., Liu, J., and Li, G. Binding modes and interaction mechanism between different base pairs and methylene blue trihydrate: a quantum mechanics study. *Advances in Experimental Medicine and Biology.* **827** 187-203 (2015).
61. Guo, Y., Chen, J., and Chen, G. A label-free electrochemical biosensor for detection of HIV related gene based on interaction between DNA and protein. *Sensors & Actuators, B: Chemical.* **184** 113-117 (2013).
62. Huang, K. J., Liu, Y. J., Wang, H. B., Wang, Y. Y., and Liu, Y. M. Sub-femtomolar DNA detection based on layered molybdenum disulfide/multi-walled carbon nanotube composites, au nanoparticle and enzyme multiple signal amplification. *Biosensors and Bioelectronics.* **55** 195-202 (2014).
63. Kong, R. M., Song, Z. L., Meng, H. M., Zhang, X. B., Shen, G. L., and Yu, R. Q.. A label-free electrochemical biosensor for highly sensitive and selective detection of DNA via a dual-amplified strategy. *Biosensors and Bioelectronics.* **54** 442-447 (2014).
64. Rashid, J. I. A., Yusof, N. A., Abdullah, J., Hashim, U., and Hajian, R. Novel Disposable Biosensor Based on SiNWs/AuNPs Modified-Screen Printed Electrode for Dengue Virus DNA Oligomer Detection. *IEEE Sensors Journal.* **15** 4420-4421 (2015).
65. Yingkajorn, M., Sermwitayawong, N., Palittapongarnpimp, P., Nishibuchi, M., Robins, W. P., Mekalanos, J. J., and Vuddhakul, V. *Vibrio parahaemolyticus* and its specific bacteriophages as an indicator in cockles (*Anadara granosa*) for the risk of *V. parahaemolyticus* infection in Southern Thailand. *Microbial Ecology.* **67** 849-856 (2014).
66. Ahmad Ganaie, H., and Ali, M. N. Short term protocol for the isolation and purification of DNA for molecular analysis. *International Journal of Pharmaceutical Sciences Review and Research.* **24** 266-270 (2014).
67. Nakano, K., Kimura, T., Kitamura, Y., Ihara, T., Ishimatsu, R., and Imato, T. Potentiometric DNA sensing platform using redox-active DNA probe pair for sandwich-type dual hybridization at indicator electrode surface. *Journal of Electroanalytical Chemistry.* **720-721** 71-75 (2014).
68. Yang, J., Jim Yang, L., Heng-Phon, T., and Gan-Moog, C. Inhibition of DNA hybridization by small metal nanoparticles. *Biophysical Chemistry.* **120** 87-95 (2006).
69. Niu, L. M., Liu, F., Wang, W., Lian, K. Q., Ma, L., Shi, H. M., and Kang, W. J. Electrochemical Behavior of Paraquat on a Highly Ordered Biosensor Based on an Unmodified DNA-3D Gold Nanoparticle Composite and Its Application. *Electrochimica Acta.* **153** 190-199 (2015).
70. Li, Z., Miao, X., Xing, K., Zhu, A., and Ling, L. Enhanced electrochemical recognition of double-stranded DNA by using hybridization chain reaction and positively charged gold nanoparticles. *Biosensors and Bioelectronics.* **74** 687-690 (2015).
71. Niu, S., Sun, J., Nan, C., and Lin, J. Sensitive DNA biosensor improved by 1,10-phenanthroline cobalt complex as indicator based on the electrode modified by gold nanoparticles and graphene. *Sensors and Actuators B: Chemical.* **176** 58-63 (2013).
72. Yi, H., Xu, W., Yuan, Y., Bai, L., Wu, Y., Chai, Y., and Yuan, R.. A pseudo triple-enzyme cascade amplified aptasensor for thrombin detection based on hemin/G-quadruplex as signal label. *Biosensors and Bioelectronics.* **54** 415-420 (2014).
73. Das, R., Sharma, M. K., Rao, V. K., Bhattacharya, B. K., Garg, I., Venkatesh, V., and Upadhyay, S. An electrochemical genosensor for *Salmonella typhi* on gold nanoparticles-mercaptosilane modified screen printed electrode. *Journal of Biotechnology.* **188** 9-16 (2014).
74. Han, X., Fang, X., Shi, A., Wang, J., and Zhang, Y. An electrochemical DNA biosensor based on gold nanorods decorated graphene oxide sheets for sensing platform. *Analytical Biochemistry.* **443** (2), 117-123 (2013).
75. Huang, K.-J., Liu, Y.-J., Zhang, J.-Z., Cao, J.-T., and Liu, Y.-M. Aptamer/Au nanoparticles/cobalt sulfide nanosheets biosensor for 17β-estradiol detection using a guanine-rich complementary DNA sequence for signal amplification. *Biosensors and Bioelectronics.* **67** 184-191 (2015).

